

DPMambaIR: All-in-One Image Restoration via Degradation-Aware Prompt State Space Model

Zhanwen Liu, Sai Zhou, Yuchao Dai, Yang Wang[†], Yisheng An, Xiangmo Zhao

Abstract—All-in-One image restoration aims to address multiple image degradation problems using a single model, offering a more practical and versatile solution compared to designing dedicated models for each degradation type. Existing approaches typically rely on Degradation-specific models or coarse-grained degradation prompts to guide image restoration. However, they lack fine-grained modeling of degradation information and face limitations in balancing multi-task conflicts. To overcome these limitations, we propose DPMambaIR, a novel All-in-One image restoration framework that introduces a fine-grained degradation extractor and a Degradation-Aware Prompt State Space Model (DP-SSM). The DP-SSM leverages the fine-grained degradation features captured by the extractor as dynamic prompts, which are then incorporated into the state space modeling process. This enhances the model’s adaptability to diverse degradation types, while a complementary High-Frequency Enhancement Block (HEB) recovers local high-frequency details. Extensive experiments on a mixed dataset containing seven degradation types show that DPMambaIR achieves the best performance, with 27.69dB and 0.893 in PSNR and SSIM, respectively. These results highlight the potential and superiority of DPMambaIR as a unified solution for All-in-One image restoration.

Keywords—All-in-One, Image Restoration, State Space Model

I. INTRODUCTION

IMAGE restoration is a fundamental task in computer vision, aiming to recover high-quality images from degraded inputs. Recent advances in deep learning have significantly improved performance in Degradation-specific restoration tasks, such as image denoising [1], [2], deblurring [3], deraining [4], dehazing [5], [6] and low-light enhancement [7]. However, traditional methods typically rely on Degradation-specific models explicitly tailored to individual degradation types. These approaches often require prior knowledge of the degradation type, which limits their practicality in real-world scenarios, such as autonomous driving and nighttime surveillance, where diverse and unknown degradations frequently coexist.

To address this limitation, recent studies explore All-in-One image restoration frameworks that unify multiple restoration tasks into a single model. Existing methods can be broadly categorized into Mixture-of-Experts (MoE)-based and Prompt-based approaches. MoE-based methods, such as MoFME [8], dynamically route tasks to specialized experts using an

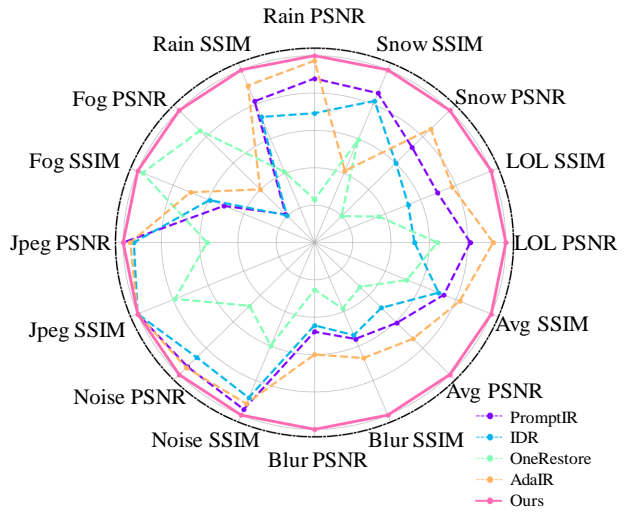


Fig. 1. Comparison with SOTA All-in-One Image Restoration Methods on mixed Dataset. Our DPMambaIR achieves consistently better performance.

uncertainty-aware router, enabling effective learning of diverse expert functions. However, these methods suffer from high computational costs, increased inference complexity as the number of experts grows, and lack explicit degradation modeling, limiting adaptability to unseen or complex degradations. Prompt-based methods, like OneRestore [9], guide restoration using degradation prompts, integrating scene descriptors via cross-attention mechanisms for flexible and adaptive strategies. While effective, these methods rely on coarse prompts that fail to capture nuanced degradation characteristics and treat prompts as static inputs, limiting their ability to adapt to varying degradation intensities or specific requirements, leading to suboptimal results.

While these methods have demonstrated success in learning multiple tasks for All-in-One image restoration, two key challenges remain unresolved. First, existing models lack a degradation extractor capable of capturing fine-grained degradation features and often rely on coarse degradation labels to guide the restoration process. For example, images with varying degrees of haze are typically assigned a single haze label, failing to capture the nuanced variations in degradation levels. This simplification leads to suboptimal restoration performance, as the model cannot adapt to the diverse characteristics of different degradations. Second, current methods struggle to balance the competing requirements of varying restoration tasks. For instance, training low-light enhancement, which focuses on restoring low-frequency contrast information, alongside deblurring, which prioritizes the recovery of fine local details. This inherent task competition makes it

[†]Corresponding author.

Zhanwen Liu, Sai Zhou, Yang Wang, Yisheng An and Xiangmo Zhao are with the School of Information Engineering, Chang'an University, Shaanxi, Xi'an 710000, China (e-mail: zwliu@chd.edu.cn; 2024124095@chd.edu.cn; ywang120@chd.edu.cn, aysm@chd.edu.cn, xmzhao@chd.edu.cn).

Yuchao Dai is with the School of Electronics and Information, Northwestern Polytechnical University, Xi'an 710072, China (e-mail: daiyuchao@gmail.com).

challenging to optimize a single network for all restoration tasks simultaneously and remains a fundamental challenge for All-in-One image restoration frameworks.

To address these challenges, we propose **DPMambaIR**, a novel All-in-One image restoration framework built upon a regression-based degradation extractor and a Degradation-Aware Prompt State Space Model (DP-SSM). Unlike prior approaches that use static or class-based prompts, our method employs a degradation extractor to generate prompt vectors that encode both semantic categories and degradation distribution characteristics. These prompts are then used to dynamically modulate the state transition, input, and output matrices of a state space model, enabling fine-grained degradation modeling and adaptive coordination across frequency bands. This mechanism allows our model to better manage task competition and enhance restoration quality across diverse degradations. Moreover, while State Space Model such as Mamba exhibit strong global modeling capabilities, they are inherently biased toward low-frequency restoration [10]. To better recover local high-frequency details, we introduce a lightweight High-Frequency Enhancement Block (HEB) as a supplementary component, which delivers performance gains while incurring only negligible computational overhead.

Extensive experiments on a mixed dataset containing seven degradation types demonstrate the superiority of DPMambaIR. As shown in Fig. 1, DPMambaIR achieves state-of-the-art performance in terms of PSNR and SSIM, outperforming existing All-in-One methods such as AdaIR and OneRestore. Moreover, DPMambaIR achieves competitive results across individual tasks, including deraining, low-light enhancement, deblurring, and dehazing, showcasing its potential as an effective and robust All-in-One image restoration solution.

The contributions of this paper are summarized as follows:

- We propose a novel degradation extractor capable of capturing fine-grained degradation features from complex degraded images. These features provide critical priors to improve the performance of All-in-One image restoration.
- We design a Degradation-aware Prompt State Space Model (DP-SSM), which enhances the long-range modeling capability of Mamba by integrating degradation priors at multiple structural levels.
- Extensive experiments on a mixed dataset containing seven types of degradation demonstrate that DPMambaIR achieves state-of-the-art performance on PSNR and SSIM metrics, outperforming existing methods. The results validate the effectiveness and superiority of the proposed approach.

II. RELATED WORK

A. All-in-One Image Restoration

Image restoration is a fundamental task in computer vision, aiming to recover high-quality images from degraded inputs. Traditional methods, such as Dark Channel Prior [11] and Color Line Prior [12], rely on handcrafted priors to model degradation but struggle with complex scenarios due to predefined assumptions. The rise of deep learning [13]

has significantly advanced tasks like such as image super-resolution [14]–[16], image denoising [1], [2], deblurring [3], deraining [4], dehazing [5], desnowing [17] and low-light enhancement [7]. These approaches, leveraging convolutional neural networks (CNN)-based [18], transformer-based [19], or diffusion-based [20] architectures, enable powerful feature learning for image restoration. However, most existing works focus on addressing a single type of degradation, which limits their applicability in real-world scenarios where images often suffer from diverse and unknown types of degradation.

Recent advancements in All-in-One image restoration frameworks focus on enhancing flexibility and efficiency by leveraging various multi-task learning techniques such as Mixture-of-Experts (MoE) and text-based or vision-based prompts to handle diverse restoration tasks. For example, AirNet [21] employs contrastive learning to extract degradation representations for guiding restoration. PromptIR [22] integrates end-to-end prompt generation and interaction to adaptively handle different degradation types, while OneRestore [9] aligns text-based degradation categories with visual features as prompts. IDR [23] uses meta-learning to decompose degradations, enabling generalization across diverse scenarios. MoFME [8], on the other hand, employs an uncertainty-aware router to dynamically assign Degradation-specific features to expert modules, allowing it to specialize in multiple tasks. Similarly, AdaIR [24] achieves adaptive restoration by decoupling degradations in the frequency domain. Additionally, methods like DA-CLIP [25] leverage the pre-trained vision-language model (VLM) for prompt extraction, but the significant computational overhead introduced by VLM limits their practical efficiency.

Despite their effectiveness, most prompt-based methods rely on coarse-grained class labels or static degradation tokens, which limits their ability to model continuous degradation distributions or adapt to image-specific degradation characteristics. In contrast, our method extracts fine-grained, regression-level degradation embeddings that encode both semantic and statistical degradation features. These embeddings are used to dynamically modulate the state-space parameters of the restoration backbone, enabling degradation-aware processing throughout the network. This facilitates better coordination across restoration tasks and reduces competition between frequency components.

B. State Space Model based Image Restoration

In Image Restoration, Convolutional Neural Networks (CNN) [13] and Transformer [19] have been widely adopted due to their strong feature extraction and representation learning capabilities. CNN excels at capturing local patterns, making them suitable for tasks requiring high spatial resolution and fine details. However, their limited receptive field often hinders their ability to model long-range dependencies, which are critical for handling global degradations. On the other hand, Transformer leverages self-attention mechanisms to capture global context effectively. Despite their success, Transformers suffer from quadratic complexity relative to the input size, making them computationally and memory-intensive.

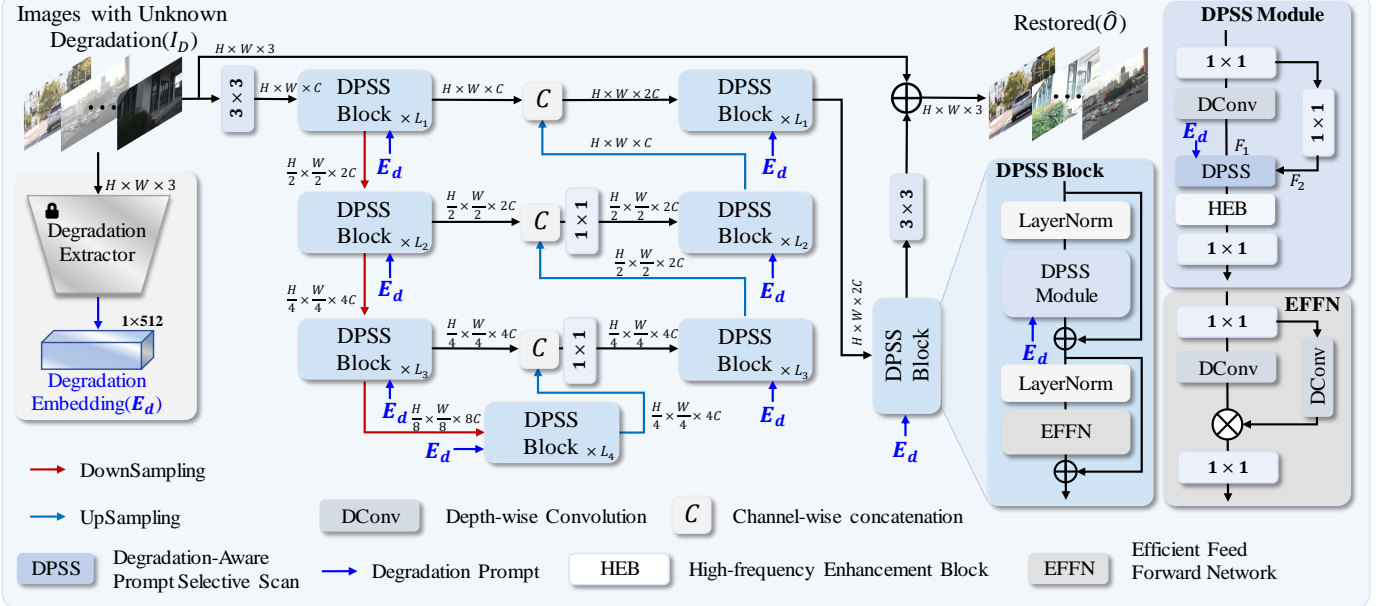


Fig. 2. The overall framework of DPMambaIR consists of a shallow feature extractor and multiple DPSS blocks, with an upsampler implemented by pixel shuffle and a downampler by pixel unshuffle. Additionally, a degradation extractor is included to extract degradation embeddings, which are then inserted into the DPSS blocks.

To address these limitations, researchers have turned to the State Space Model (SSM) [26], which provides an efficient framework for modeling long-range dependencies with linear computational complexity. Formally, SSM maps an input sequence $x(t)$ to an output sequence $y(t)$ through an implicit latent state $h(t) \in \mathbb{R}^N$, represented by a linear ordinary differential equation:

$$\begin{aligned} h'(t) &= Ah(t) + Bx(t), \\ y(t) &= Ch(t) + Dx(t). \end{aligned} \quad (1)$$

where $A \in \mathbb{R}^{N \times N}$, $B \in \mathbb{R}^{N \times 1}$, $C \in \mathbb{R}^{1 \times N}$, and $D \in \mathbb{R}$. After discretization with step size Δ , the dynamic equation can be expressed as:

$$\begin{aligned} h_i &= \bar{A}h_{i-1} + \bar{B}x_i, \\ y_i &= Ch_i + Dx_i. \end{aligned} \quad (2)$$

where $\bar{A} = \exp(\Delta A)$ and $\bar{B} = (\Delta A)^{-1}(\exp(\Delta A) - I)\Delta B$.

The introduction of Vision Mamba [27] marked the first effort to incorporate SSM into vision tasks. By proposing the Vision State Space Module (VSSM), it extended SSM to visual applications and demonstrated superior performance over Vision Transformer (ViT) [28], while maintaining lower complexity. This success inspired extensive research into SSM across diverse tasks such as object detection [29], semantic segmentation [30], and image classification [31].

In the context of Image Restoration, MambaIR [32] pioneered the integration of SSM, leveraging its linear complexity and long-range modeling capability to achieve significant improvements in both computational efficiency and perceptual quality. This was followed by several variants targeting specific restoration tasks [33]–[35], collectively showcasing the strong potential of SSM in this domain. Existing approaches typically unfold 2D images into 1D sequences and apply sequential causal modeling. However, this design still faces two limitations: **(a) Limited Global Context Utilization:** The i -th pixel

can only access the previous $i - 1$ pixels in the sequence, restricting the effective use of global context. Parallel multi-directional scanning has been explored to enlarge the receptive field, but it increases computational cost while providing limited gains in low-level vision tasks [32]. **(b) Lack of Effective Degradation-Aware Mechanisms:** Current SSM-based methods primarily target single-task restoration. Their transition and output mappings are fixed or solely input-driven, without leveraging external degradation priors. As a result, they cannot dynamically adapt to diverse degradation types or levels, leading to suboptimal performance in All-in-One image restoration task.

These limitations motivate the introduction of a degradation-aware modulation mechanism into the SSM pipeline. In this work, we propose a Degradation-aware Prompt State Space Model (DP-SSM), where degradation embeddings dynamically modulate the state-space transition and output matrices. This design enables a fine-grained, task-aware mechanism that balances global modeling with degradation-specific guidance, enhancing the flexibility and effectiveness of SSM for complex restoration scenarios.

III. METHOD

A. Problem Definition

All-in-One Image Restoration aims to address a wide range of image degradation types within a unified framework. Specifically, given a degraded image $\mathbf{I}_D \in \mathbb{R}^{3 \times H \times W}$, where D denotes the degradation process, our goal is to restore the clean image $\hat{\mathbf{O}} \in \mathbb{R}^{3 \times H \times W}$ using a unified model \mathcal{F} . This can be formulated as:

$$\hat{\mathbf{O}} = \mathcal{F}(\mathbf{I}_D). \quad (3)$$

where \mathcal{F} is designed to generalize across various degradation types, such as noise, blur, compression artifacts, and weather

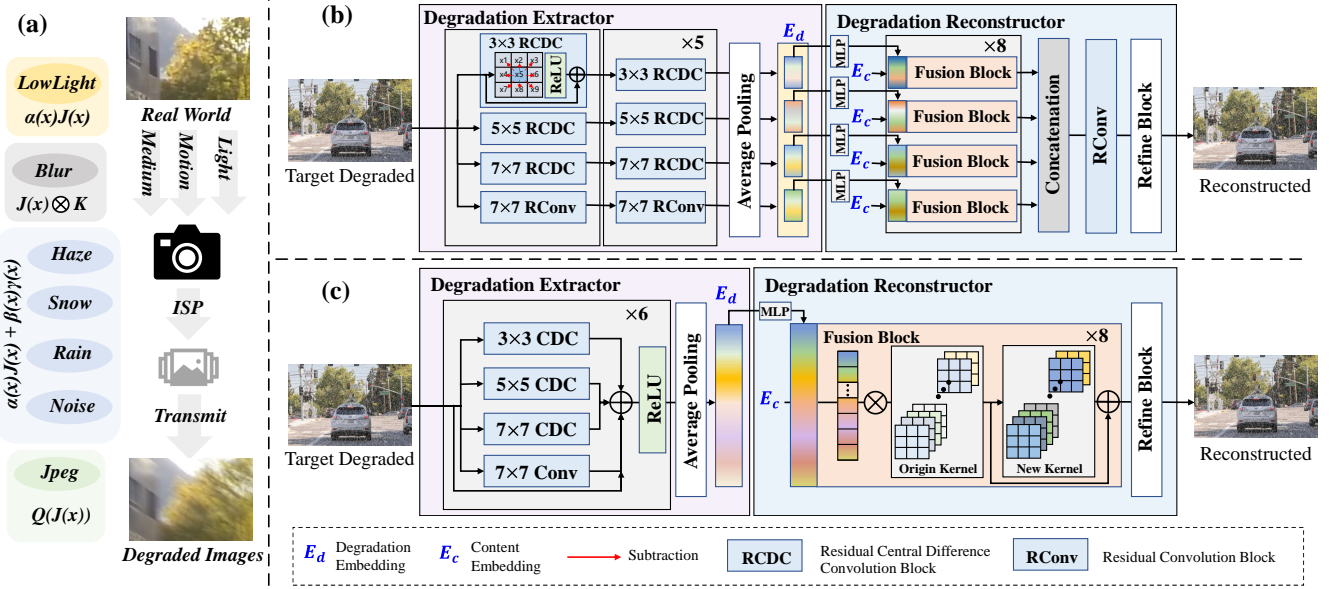


Fig. 3. (a) Real-World Image Degradation Modeling Process. (b) Architecture details of the Large version degradation extractor and reconstructor. (c) Architecture details of the normal version degradation extractor and reconstructor.

effects, without explicit knowledge of Deg . The degradation process Deg can be mathematically represented as:

$$\mathbf{I}_D = Deg(\mathbf{I}_C) + \eta. \quad (4)$$

Here, $\mathbf{I}_C \in \mathbb{R}^{3 \times H \times W}$ denotes the original clean image, Deg represents the degradation operator (e.g., blur kernel, brightness, or quality compression), and η signifies additive noise. The main challenge arises from the fact that Deg is usually unknown and varies across tasks, making it difficult to design a universal model capable of effectively handling all possible degradations.

Unlike degradation-specific restoration, the All-in-One setting requires the model to generalize across a broad spectrum of degradation types without prior knowledge of degradation parameters. This introduces two main challenges: (a) how to represent fine-grained degradation information in a unified way; and (b) how to dynamically adapt the model behavior based on such information during inference.

B. DPMambaIR

We propose **DPMambaIR**, a degradation-aware framework for All-in-One image restoration. As illustrated in Fig. 2, we first establish a Mamba-based image restoration baseline using an asymmetric encoder-decoder design within a U-shaped architecture. The restoration process begins with a 3×3 convolutional layer, which extracts shallow features $\mathbf{F} \in \mathbb{R}^{H \times W \times C}$ from the degraded image. These features then pass through three encoding stages, each followed by downsampling. During each encoding stage, the resolution of the feature map is halved while the number of channels is doubled. Subsequently, the features pass through three decoding stages, where each stage involves upsampling and concatenating the output of the decoder with the corresponding output of the encoder to form the input for the next decoding stage. Finally, after a refinement stage, the clean image is

restored through a shortcut connection that combines the input degraded image with the output of the decoder.

To address the challenges posed by unknown degradation types and levels in All-in-One image restoration tasks, we propose a *Degradation Extractor* pre-trained using degraded image reconstruction. This model compresses degradation type and severity information into a compact embedding, enabling the model to transition from blind to non-blind image restoration through finer-grained degradation representation. To further optimize the utilization of the extracted degradation embedding, we revisit the selective state-space modeling process. Specifically, we propose a *Degradation-Aware Prompt State Space Model*, which guides the image restoration process by compressing historical information and supplementing global degradation information.

C. Degradation Extractor

To better extract degradation information from images, we revisit the degradation modeling process of real-world images, which spans from image capture and imaging to transmission, as illustrated in Fig. 3 (a). This process typically involves four common types of degradations: (1) poor illumination conditions, (2) relative motion between the target objects and the camera, (3) artifacts introduced by transmission media in the optical path, and (4) compression during storage and transportation. We unify these scenarios into a generalized degradation formation model:

$$I(x) = Q((\alpha(x)J(x) + \beta(x)\gamma(x)) \otimes K). \quad (5)$$

where $J(x)$ represents the clean image, $\alpha(x)$ models the luminance adjustment, such as the effects of insufficient lighting in low-light or adverse weather conditions (e.g., rain or fog), and $\gamma(x)$ accounts for artifacts caused by occlusions from aerosols, raindrops, or snow particles in the transmission medium. $\beta(x)$ modulates $\gamma(x)$ based on varying spatial properties, K

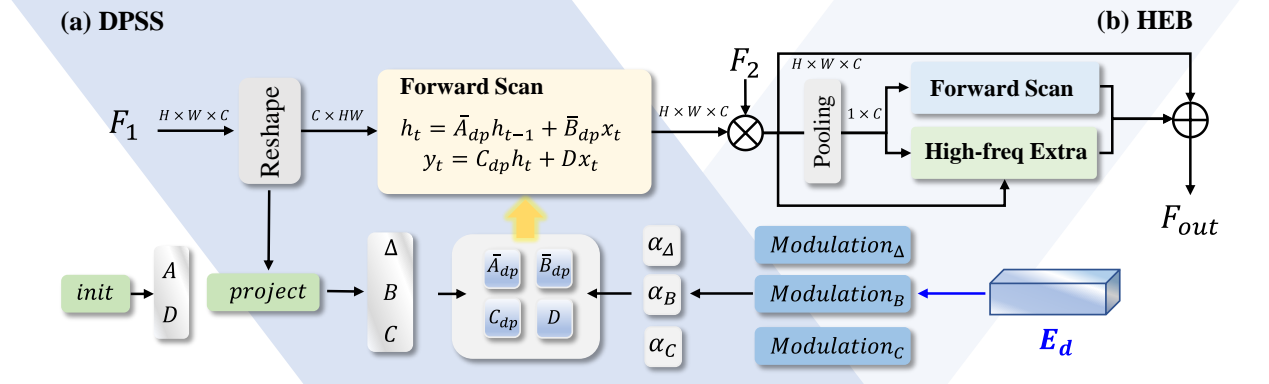


Fig. 4. The Architecture of (a) Degradation-aware Prompt Selective Scan (DPSS) and (b) High-frequency Enhancement Block (HEB), with Three Inputs F_1 , F_2 , and Degradation Embedding E_d .

represents the blur introduced by relative motion between the target and the camera, and Q denotes the compression applied during storage and transmission.

Based on the aforementioned degradation modeling process, we design a universal degradation extractor, as illustrated in Fig. 3 (b). Specifically, we introduce central difference convolution (CDC) [36]–[38] to extract edge and texture degradation cues related to illumination and blur. In addition, we propose a multi-scale degradation perception module, which employs four parallel CDC operators of different sizes to capture degradation features at various scales. By concatenating the outputs, the module retains complete degradation representations across all frequency components. Furthermore, we employ three groups of CDC with different scales to capture artifacts of varying sizes, such as visual artifacts and snowflakes. Additionally, we integrate a traditional convolution branch to learn brightness-related representations.

To achieve a balance between extraction performance and computational cost, we introduce a re-parameterization technique for efficient integration of degradation representations, as illustrated in Fig. 3 (c). These two implementations correspond to different variants of our method, which are presented in Table I as DPMambaIR-L and DPMambaIR, respectively.

Furthermore, to endow the degradation extractor with fine-grained degradation encoding capability, we propose a pre-training strategy based on degraded image reconstruction. This strategy leverages a hybrid dataset composed of paired samples with diverse degradation types. The key objective is to train the degradation extractor \mathcal{E} to capture detailed degradation information from a degraded image I_D and compress it into a compact embedding E_d , formulated as:

$$E_d = \mathcal{E}(I_D). \quad (6)$$

Subsequently, the reconstruction unit \mathcal{R} takes E_d together with the clean content embedding E_c to reconstruct the degraded image I_D . In particular, we adopt Restormer as the content extractor to derive E_c from the clean reference image O , expressed as:

$$E_c = \text{Restormer}(O), \quad \hat{I}_D = \mathcal{R}(E_c, E_d). \quad (7)$$

This pretraining paradigm encourages the degradation extractor to encode both the type and severity of degradation into

a continuous embedding space, which then serves as a compact and informative task descriptor for downstream restoration. We further introduce a dual-component loss function L , which combines the L_1 norm and the Learned Perceptual Image Patch Similarity (LPIPS) metric. The combined loss function is expressed as $L(I_D, \hat{I}_D) = L_1 + L_{LPIPS}$, striking a balance between reconstruction accuracy and perceptual quality.

D. Degradation-aware Prompt State Space Model

To address the limitations of SSM-based image restoration—specifically the insufficient use of global context and the lack of effective degradation-aware mechanisms, we propose a novel Degradation-aware Prompt State Space Model (DP-SSM) to fully unlock the potential of SSM in All-in-One image restoration. Specifically, we propose a novel Degradation-aware Prompt Selective Scan, which incorporates degradation information into the State Space Model. This is achieved by leveraging a Degradation Embedding extracted from a pre-trained Degradation Extractor to provide supplementary degradation-related contextual information that the traditional SSM cannot capture. In addition, we modulate the parameter matrices in the state-space equations to establish a degradation-aware mechanism. This mechanism enables SSM to adapt to multi-task learning and handle task competition. To better recover local high-frequency details, we design a lightweight High-frequency Enhancement Block (HEB). This component ensures the preservation of high-frequency details and enhances the overall model performance.

Degradation-aware Prompt Selective Scan. We revisit the traditional SSM, whose parameter settings are shown in Eq.(2). Matrices A , B , C , and D control the SSM output. The state transition matrix A compresses historical information, while the input matrix B maps input signals to the state space, determining their influence on historical states. The output matrix C maps historical states to the observable space, reflecting their impact on the output. Matrix D provides a direct pathway from input to output, similar to a residual connection. In traditional SSM, these matrices and Δ are derived from:

$$\begin{aligned} A &= \text{init}(), D = \text{init}(), \\ B &= \text{Linear}(x), C = \text{Linear}(x), \Delta = \text{Linear}(x). \end{aligned} \quad (8)$$

where $init()$ is an initialization method that does not depend on the input x . However, such parameterization does not incorporate degradation information, which motivates us to introduce a degradation-aware prompt mechanism to guide the state-space modeling.

To integrate degradation awareness into the SSM, we first utilize a degradation extractor \mathcal{E} to extract the degradation embedding \mathbf{E}_d from the input image I_D . This embedding is then employed to modulate Δ , the input matrix B , and the output matrix C , thereby enhancing the model's ability to compress historical information, process input signals, and capture global context, as illustrated in Fig. 4 (a). The specific formulation is given as follows:

$$\begin{aligned} \mathbf{E}_d &= \mathcal{E}(I_D), \\ \alpha_\Delta &= \mathcal{M}_\Delta(\mathbf{E}_d), \alpha_B = \mathcal{M}_B(\mathbf{E}_d), \alpha_C = \mathcal{M}_C(\mathbf{E}_d), \\ \Delta_{dp} &= \alpha_\Delta \cdot \Delta, B_{dp} = \alpha_B \cdot B, C_{dp} = \alpha_C \cdot C. \end{aligned} \quad (9)$$

Here, \mathcal{M}_Δ , \mathcal{M}_B , and \mathcal{M}_C are combinations of linear layers used to map the degradation embedding \mathbf{E}_d into feature spaces, forming modulation vectors α_Δ , α_B , and α_C for Δ , B , and C , respectively. Δ_{dp} , B_{dp} , and C_{dp} are the newly modulated SSM parameters.

Finally, the formulation of the Degradation-aware State Space Model can be expressed as follows:

$$\begin{aligned} \bar{A}_{dp} &= \exp(\Delta_{dp} A), \\ \bar{B}_{dp} &= (\Delta_{dp} A)^{-1}(\exp(A) - I) \cdot \Delta_{dp} B_{dp}, \\ h_i &= \bar{A}_{dp_i} h_{i-1} + \bar{B}_{dp_i} x_i, \\ y_i &= C_{dp} h_i + D x_i. \end{aligned} \quad (10)$$

Through this approach, the transformation matrix A and input matrix B gain degradation-aware capabilities, integrating degradation cues of various types and levels during historical information compression and input signal processing, making the model more task-friendly. The output matrix C controls how historical information affects the output. In traditional SSM, the i -th pixel can only observe the $i-1$ preceding pixels, leading to a limited global receptive field. While existing methods address this with parallel multi-directional scanning, this increases computational costs and offers limited performance gains in low-level vision tasks [32]. Instead, we retain single-directional scanning and enhance global degradation cues via C , achieving efficient global awareness with lower computational overhead.

High-frequency Enhancement Block. All-in-One image restoration involves recovering image components distributed across different frequency bands. While our proposed Degradation-aware Prompt State Space Model enables dynamic adaptation to degradation characteristics and partially alleviates inter-task conflicts, it still exhibits a bias toward low-frequency restoration due to the inherent global modeling nature of Mamba. As shown in Fig. 5, All-in-One models tend to underperform in reconstructing high-frequency details such as edges and textures, compared to degradation-specific models. To address this limitation, we introduce an extremely lightweight High-Frequency Enhancement Block (HEB) as a complementary module.

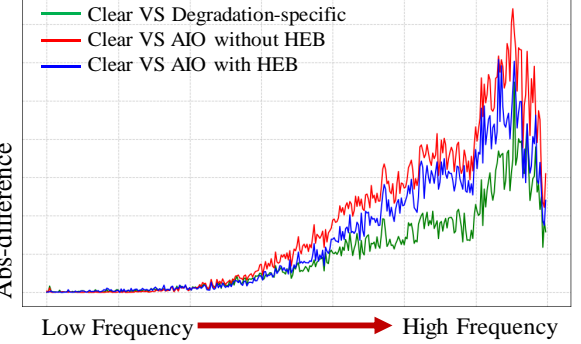


Fig. 5. We compare frequency-domain differences between clear and restored images under three configurations. The All-in-One setting shows a notable high-frequency gap compared to the Degradation-specific setting, which is significantly reduced by adding the High-frequency Enhancement Block (HEB), as shown by the blue line.

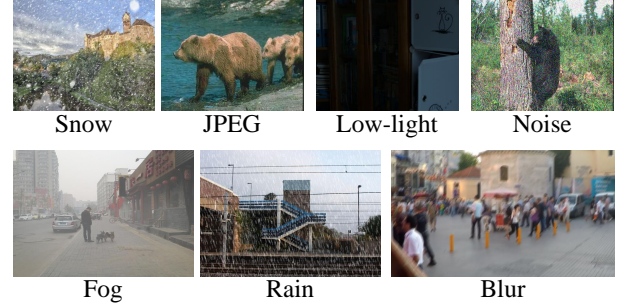


Fig. 6. Examples of Seven Types of Image Degradations in the Dataset.

For input features F , we first extract channel-wise low-frequency features using global average pooling, then subtract them from F to obtain high-frequency components, as illustrated in Fig. 4(b). Finally, the high-frequency features are added back to enhance F , formulated as:

$$F_{enhanced} = F + \alpha \cdot (F - \mathcal{G}(F)). \quad (11)$$

Here, α represents a learnable scalar that controls the contribution of high-frequency enhancement, and \mathcal{G} denotes the global average pooling operation. $F_{enhanced}$ is the enhanced feature map.

E. Loss Function

We employ the commonly used L1 loss \mathcal{L}_1 and L2 loss \mathcal{L}_2 in low-level vision tasks. Additionally, following previous works [39], [40], we incorporate a frequency-domain loss \mathcal{L}_{fft} for training. The total loss is defined as:

$$\mathcal{L}_{total} = \lambda_1 \cdot \mathcal{L}_1(O, \hat{O}) + \lambda_2 \cdot \mathcal{L}_2(O, \hat{O}) + \lambda_3 \cdot \mathcal{L}_{fft}(O, \hat{O}). \quad (12)$$

where O and \hat{O} denote the model output and the ground truth, respectively. The parameters λ_1 , λ_2 , and λ_3 are balancing factors, which we set to 1, 0.5 and 0.001, respectively.

IV. EXPERIMENT AND ANALYSIS

We evaluate our method on both All-in-one image restoration tasks and Degradation-specific image restoration tasks. In the All-in-One Image Restoration setting, we train a single model on a dataset containing seven types of degradation. For Degradation-specific image restoration, we train separately on datasets corresponding to each type of degradation.

TABLE I

QUANTITATIVE COMPARISON ON SEVEN DATASETS FOR ALL-IN-ONE IMAGE RESTORATION TASK WITH STATE-OF-THE-ART METHODS. THE BEST AND SECOND-BEST RESULTS ARE IN **BOLD** AND UNDERLINE.

Method	Lowlight		Snow		Rain		Haze		Jpeg		Noise		Blur		Average	
	PSNR	SSIM														
MPRNet	19.71	0.659	30.94	0.938	26.27	0.912	25.63	0.947	30.51	0.938	28.03	0.897	26.07	0.869	26.74	0.880
MIRNet	19.81	0.668	31.04	0.941	25.77	0.907	22.26	0.882	30.54	0.939	28.14	0.900	26.32	0.873	26.27	0.873
NAFNet	19.49	0.650	30.33	0.935	26.04	0.906	25.63	0.946	30.20	0.936	27.80	0.895	26.13	0.870	26.52	0.877
Restormer	19.99	0.670	31.67	0.944	26.91	0.919	26.18	0.953	30.56	0.939	28.17	0.890	26.62	0.880	27.16	0.886
MambaIR	19.81	0.664	30.43	0.935	25.52	0.901	25.90	0.944	30.38	0.937	27.91	0.895	26.07	0.869	26.57	0.878
PromptIR	19.90	0.669	31.52	0.943	26.80	0.918	26.13	0.945	30.57	0.939	28.18	0.901	26.36	0.874	27.07	0.884
IDR	19.68	0.663	31.16	0.941	26.39	0.914	26.11	0.948	30.51	0.939	28.10	0.899	26.29	0.873	26.89	0.883
NDR-Restore	19.79	0.635	30.00	0.902	26.00	0.813	27.00	0.943	30.19	0.872	27.78	0.786	25.77	0.791	26.64	0.820
OneRestore	19.77	0.657	29.95	0.931	25.37	0.900	27.74	0.962	30.10	0.934	27.65	0.890	25.90	0.866	26.64	0.877
MoCEIR	19.92	0.674	31.22	0.943	26.56	0.920	28.06	0.963	30.51	0.939	28.13	0.900	26.34	0.874	27.25	0.888
AdaIR	19.99	0.672	31.94	0.923	27.01	0.922	26.61	0.952	30.53	0.939	28.19	0.900	26.61	0.879	27.26	0.887
DPMambaIR	20.04	0.680	32.36	0.949	27.07	0.926	28.13	0.963	30.57	0.939	28.25	0.902	27.43	0.894	27.69	0.893
DPMambaIR-L	20.06	0.677	32.31	0.950	27.11	0.925	28.39	0.963	30.55	0.939	28.21	0.902	27.45	0.895	27.73	0.893

TABLE II

QUANTITATIVE COMPARISON ON DERAINING, LOW-LIGHT IMAGE ENHANCEMENT(LLIE), DEBLURRING AND DEHAZING FOR DEGRADATION-SPECIFIC IMAGE RESTORATION TASK WITH STATE-OF-THE-ART METHODS. THE BEST AND SECOND-BEST RESULTS ARE IN **BOLD** AND UNDERLINE.

Deraining	PSNR	SSIM	LLIE	PSNR	SSIM	Deblurring	PSNR	SSIM	Dehazing	PSNR	SSIM
JORDER	26.25	0.835	EnlightenGAN	17.61	0.653	DeepDeBlur	29.08	0.913	GCANet	26.59	0.935
PReNet	29.46	0.899	MIRNet	<u>24.14</u>	0.830	DeBlurGAN	28.70	0.858	GridDehazeNet	25.86	0.944
MPRNet	30.41	0.891	URetinex-Net	19.84	0.824	DeBlurGANV2	29.55	0.934	DeHazeFormer	30.29	0.964
MAXIM	30.81	0.903	MAXIM	23.43	0.863	MT-RNN	<u>31.15</u>	<u>0.945</u>	MAXIM	29.12	0.932
Restormer	31.46	0.904	IAT	23.38	0.809	IR-SDE	30.70	0.901	DA-CLIP	30.16	0.936
OneRestore	29.36	0.944	OneRestore	22.97	0.835	OneRestore	28.76	0.915	OneRestore	30.16	0.974
MoCEIR	31.23	0.960	MoCEIR	23.64	0.818	MoCEIR	30.05	0.933	MoCEIR	30.62	0.975
AdaIR	31.46	0.961	AdaIR	23.47	0.831	AdaIR	30.57	0.939	AdaIR	<u>30.87</u>	<u>0.975</u>
DPMambaIR	32.30	0.967	DPMambaIR	24.20	<u>0.852</u>	DPMambaIR	31.42	0.948	DPMambaIR	30.89	0.977

A. Experimental Settings

Training Details. Building on previous works [22], [32], [39], we develop a Mamba-based baseline for image restoration. Our method is trained using the AdamW [41] optimizer with parameters $\beta_1 = 0.9$, $\beta_2 = 0.999$, and a weight decay of $3e^{-4}$ for 300,000 iterations. The initial learning rate of $3e^{-4}$ is gradually reduced to $1e^{-6}$ through cosine annealing. Following [39], we employ a progressive training strategy, cropping image patches of size 192×192 . Horizontal and vertical flips are applied for data augmentation. Our experiments are conducted on a single NVIDIA RTX A100 GPU and implemented using the PyTorch platform.

Datasets. For All-in-One image restoration, we collect a large-scale mixed dataset covering seven common degradation types: haze, rain, snow, low-light, blur, noise, and JPEG compression, as shown in Fig. 6. Detailed information regarding these datasets is summarized in Table III. Additionally, degradation-specific evaluations are conducted using LOL [42] for low-light enhancement, GoPro [43] for deblurring, Rain100H [44] for deraining, and RESIDE6K [45] for dehazing.

Evaluation Metrics. Following previous works [32], [39], we use peak signal-to-noise ratio (PSNR) and structural similarity index measure (SSIM) to quantitatively compare different methods on the RGB channels.

Comparisons with State-of-the-art Methods. For All-in-One image restoration, we compare against eleven methods: MIRNet [51], NAFNet [52], MPRNet [53], Restormer [39], MambaIR [32], PromptIR [22], IDR [23], NDR-Restore [54], OneRestore [9], MoCEIR [55], and AdaIR [24]. The first four are general-purpose restoration models, while the latter four are designed specifically for All-in-One restoration: Prompt-

TABLE III
DATASETS FOR IMAGE RESTORATION TASKS

Degradation	Dataset	Train Pairs	Test Pairs
Haze	RESIDE6K [45]	6000	1000
Rain	Rain13K [46]	13711	-
	Rain100H [44]	-	100
Snow	Snow100K [47]	5000	1000
Low Light	LOL [42], LSRW [48]	6085	65
Blur	GoPro [43]	2103	1111
Noise	WaterlooED [49]	4744	-
	BSD400 [50]	-	400
JPEG	WaterlooED [49]	4744	-
	BSD400 [50]	-	400

tIR uses visual prompts, OneRestore employs a pre-trained degradation encoder with cross-attention, and AdaIR leverages frequency-domain information for adaptive restoration. For degradation-specific restoration, we also include representative single-task methods such as JORDER [56] (deraining), MAXIM [57] (deblurring), EnlightenGAN [58] (low-light enhancement), DeepDeblur [59], AdaIR [24], DA-CLIP [25], among others.

B. Quantitative Results

All-in-one Image Restoration. We conducted two versions of our method for comparison: the normal version (DPMambaIR) and a Large version (DPMambaIR-L). The normal version adopts the degradation extractor illustrated in Fig. 3(c), while the Large version uses the architecture shown in Fig. 3(b). For subsequent evaluations, we primarily adopt the normal version unless otherwise specified. We compare our method against eleven state-of-the-art image restoration approaches. As shown in Table I, for the All-in-One image restoration

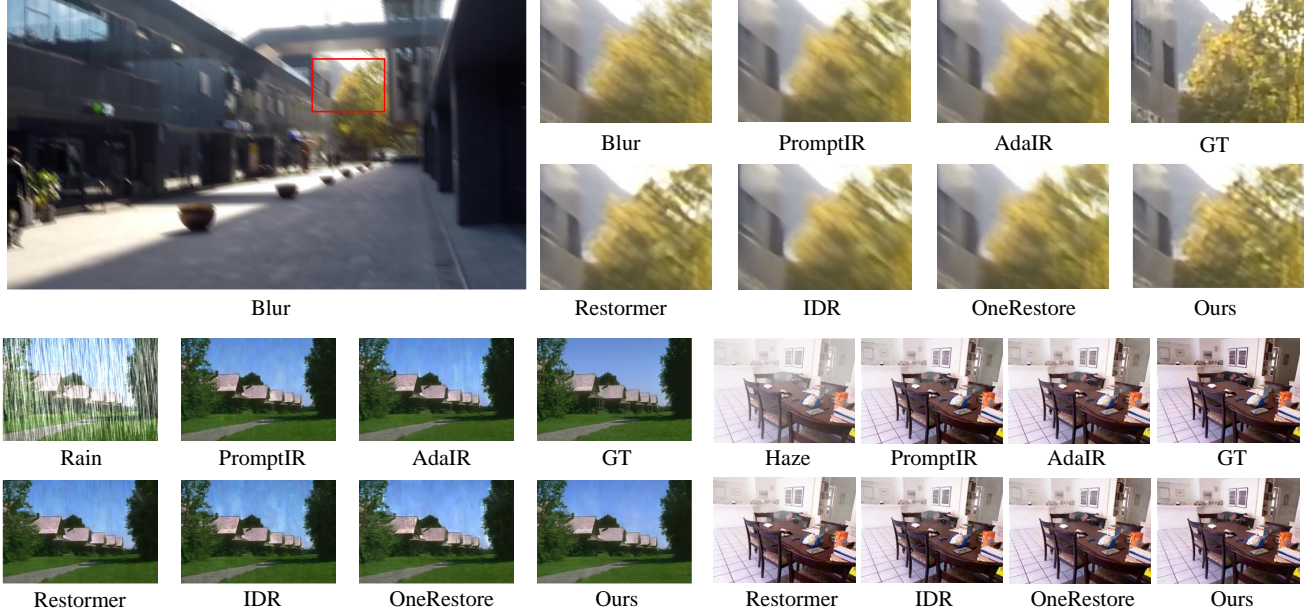


Fig. 7. Qualitative comparison on Deblurring, Deraining and Dehazing for All-in-One Image Restoration Task.

task, our method achieves the best PSNR and SSIM on the aforementioned mixed datasets, outperforming existing methods. Specifically, our method achieves a PSNR of 27.69dB and an SSIM of 0.893, surpassing AdaIR by 0.43dB and 0.011, respectively. Additionally, DPMambalIR-L achieves a PSNR of 27.73dB and an SSIM of 0.893, slightly outperforming the normal version.

We achieve the best performance across all seven sub-tasks. Experimental results indicate that multi-task learning often encounters challenges in balancing performance across different tasks. For instance, AdaIR demonstrates strong performance in deraining but performs poorly in dehazing. On the other hand, OneRestore excels in dehazing but delivers suboptimal results in tasks such as deraining and deblurring. In contrast, our method effectively tackles the balance issue in multi-task learning, achieving consistently optimal performance across all sub-tasks. These findings highlight the effectiveness and superiority of our proposed method.

Degradation-Specific Image Restoration. We evaluate our method on four Degradation-specific tasks, consistently achieving superior performance across multiple datasets compared to state-of-the-art CNN-based, transformer-based, and diffusion-based approaches, as shown in Table II. On Rain100H [44], our method achieves a PSNR of 32.30dB and SSIM of 0.967, surpassing AdaIR by 0.84dB and 0.006, respectively. On the LOL dataset [42], it achieves 24.20dB PSNR and 0.852 SSIM, outperforming MIRNet by 0.06dB and 0.022. For deblurring on GoPro [43], it attains 31.42dB PSNR and 0.948 SSIM, exceeding MT-RNN by 0.27dB and 0.003. On RESIDE6K [45], it achieves 30.89dB PSNR and 0.973 SSIM, outperforming AdaIR by 0.02dB and 0.002. These results highlight the versatility and effectiveness of our method in addressing diverse degradation restoration tasks.

C. Qualitative Results

Fig. 7 presents the visual results of deblurring, deraining, and dehazing under the All-in-One Image Restoration task setting. Our method demonstrates superior visual performance compared to other approaches. Specifically, in deblurring, our method restores sharper edge details; in deraining, it more effectively removes rain streaks while recovering background information; and in dehazing, it focuses on regions often overlooked by other methods, resulting in more comprehensive dehazing performance. Additional visual comparisons under both the All-in-One and Degradation-specific settings are provided in the Appendix.

D. Ablation Study

We conduct ablation studies to evaluate our key designs: the degradation-aware prompts and High-frequency Enhancement Block (HEB) (Table IV), degradation extraction and utilization methods (Table V), and the global information supplementation strategy (Table VI).

Table IV shows the effectiveness of our core modules. The High-frequency Enhancement Block (HEB) alone improves the baseline by 0.29 dB PSNR by enhancing local details. Degradation-aware prompts (P_Δ, P_B) bring a more significant gain of 0.64 dB, showing the benefit of adaptive modulation. Adding P_C for global cues offers further slight improvement. The full model demonstrates the synergy between prompt-based modulation and frequency enhancement, achieving the best performance.

Table V presents the results for degradation extraction and utilization methods. For degradation extraction, we compare three approaches: (1) “Classes”, which provides manually specified degradation types and can be regarded as a 100% accurate non-blind setting; (2) a pre-trained degradation classifier from OneRestore [9]; and (3) our fine-grained degradation representation via image reconstruction. The OneRestore

TABLE IV
ABLATION STUDIES ON OUR PROPOSED CORE MODULES.

Method	P_Δ	P_B	P_C	HEB	PSNR	SSIM
Baseline	✗	✗	✗	✗	26.96	0.884
(a)	✗	✗	✗	✓	27.25	0.887
(b)	✓	✓	✗	✗	27.60	0.892
(c)	✓	✓	✓	✗	27.67	0.893
(d)	✓	✓	✓	✓	27.69	0.893

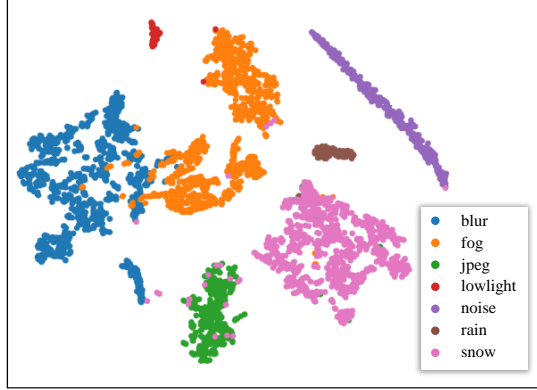


Fig. 8. t-SNE visualization of degradation embeddings.

extractor, optimized for classification, is insensitive to degradation strength or location, leading to poorer results. Our method surpasses the non-blind "Classes" baseline by 0.11 dB PSNR.

Fig. 8 visualizes the t-SNE embeddings of the extracted degradation features. Significant gaps exist between different degradation types, indicating clear separability. Notably, although JPEG and noise share the same content during synthesis, the t-SNE visualization reveals that their separability is primarily driven by degradation information rather than image content.

For degradation utilization, we compare concatenation and attention-based fusion with our prompt modulation design. Our prompt-based modulation outperforms simple concatenation or attention-based fusion, showing better adaptability to local degradations.

Table VI presents the ablation study on global information supplementation. We compare our Prompt-C with Mamba's bi-directional scanning scheme. Compared to Mamba's bi-directional scan, our Prompt-C not only achieves slightly better performance but is also more efficient, reducing GFLOPs by nearly 37% (Table VI). This highlights its effectiveness as a lightweight global information supplementation method.

TABLE V
ABLATION STUDY ON DIFFERENT DEGRADATION EXTRACTION AND UTILIZATION METHODS.

Comparison Projects	Method	PSNR	SSIM
Degradation Extraction	Classes	27.58	0.892
	OneRestore*	27.56	0.891
	Ours	27.69	0.893
Degradation Insertion	Concat	26.96	0.882
	Attention	27.39	0.882
	Ours	27.69	0.893

TABLE VI
ABLATION STUDY ON DIFFERENT METHODS FOR GLOBAL INFORMATION SUPPLEMENTATION.

Method	PSNR	SSIM	Params(M)	GFLOPs
Bi-direction Scan	27.66	0.893	31.43	244.3
Prompt Matrix C (Ours)	27.69	0.893	29.35	153.3

V. CONCLUSION

We propose DPMambaIR, a novel All-in-One framework for image restoration capable of handling diverse degradation types. The core of our framework is a Degradation-Aware Prompt State Space Model (DP-SSM) that leverages a fine-grained degradation extractor. This design enables the dynamic integration of degradation features into the state-space modeling process, allowing for adaptive handling of complex degradation scenarios while maintaining global degradation awareness. Furthermore, a lightweight High-frequency Enhancement Block (HEB) was introduced to complement the main framework by enhancing high-frequency details restoration with negligible computational overhead. This study underscores the importance of fine-grained degradation modeling and dynamic feature modulation in advancing All-in-One image restoration frameworks. Extensive experiments on a mixed dataset containing seven degradation types show that DPMambaIR achieves the best performance, establishing it as a promising approach for unified image restoration.

REFERENCES

- [1] T. Zhang, R. Wang, Y. Niu, Z. Li, and T. Zhao, "Hugs-net: A lightweight and unified network for adverse weather image denoising," *IEEE Transactions on Multimedia*, pp. 1–10, 2025.
- [2] C. Kim, T. H. Kim, and S. Baik, "Lan: Learning to adapt noise for image denoising," in *Proceedings of the IEEE/CVF Conference on Computer Vision and Pattern Recognition*, 2024, pp. 25193–25202.
- [3] K. Zhuang, Q. Li, Y. Yuan, and Q. Wang, "Multi-domain adaptation for motion deblurring," *IEEE Transactions on Multimedia*, vol. 26, pp. 3676–3688, 2024.
- [4] Y.-T. Peng, W.-H. Li, and Z. Chen, "Rain2avoid: Learning deraining by self-supervision," *IEEE Transactions on Multimedia*, vol. 27, pp. 4765–4779, 2025.
- [5] Y. Su, N. Wang, Z. Cui, Y. Cai, C. He, and A. Li, "Real scene single image dehazing network with multi-prior guidance and domain transfer," *IEEE Transactions on Multimedia*, vol. 27, pp. 5492–5506, 2025.
- [6] Z. Wang, H. Zhao, J. Peng, L. Yao, and K. Zhao, "Odr: Orthogonal decoupling contrastive regularization for unpaired image dehazing," in *Proceedings of the IEEE/CVF Conference on Computer Vision and Pattern Recognition*, 2024, pp. 25479–25489.
- [7] I. Morawski, K. He, S. Dangi, and W. H. Hsu, "Leveraging content and context cues for low-light image enhancement," *IEEE Transactions on Multimedia*, vol. 27, pp. 5337–5351, 2025.
- [8] R. Zhang, Y. Luo, J. Liu, H. Yang, Z. Dong, D. Gudovskiy, T. Okuno, Y. Nakata, K. Keutzer, Y. Du *et al.*, "Efficient deweather mixture-of-experts with uncertainty-aware feature-wise linear modulation," in *Proceedings of the AAAI Conference on Artificial Intelligence*, vol. 38, no. 15, 2024, pp. 16812–16820.
- [9] Y. Guo, Y. Gao, Y. Lu, H. Zhu, R. W. Liu, and S. He, "Onerestore: A universal restoration framework for composite degradation," in *European Conference on Computer Vision*. Springer, 2024, pp. 255–272.
- [10] X. Ma, Z. Ni, and X. Chen, "Tinyvim: Frequency decoupling for tiny hybrid vision mamba," *arXiv preprint arXiv:2411.17473*, 2024.
- [11] K. He, J. Sun, and X. Tang, "Single image haze removal using dark channel prior," *IEEE transactions on pattern analysis and machine intelligence*, vol. 33, no. 12, pp. 2341–2353, 2010.
- [12] R. Fattal, "Dehazing using color-lines," *ACM transactions on graphics (TOG)*, vol. 34, no. 1, pp. 1–14, 2014.
- [13] Y. LeCun, Y. Bengio, and G. Hinton, "Deep learning," *nature*, vol. 521, no. 7553, pp. 436–444, 2015.

[14] S. Liu, D. Suzhang, M. Yang, X. Zheng, and C. Zhu, "Depth map super-resolution via deep cross-modality and cross-scale guidance," *IEEE Transactions on Multimedia*, pp. 1–14, 2025.

[15] L. Peng, W. Li, R. Pei, J. Ren, J. Xu, Y. Wang, Y. Cao, and Z.-J. Zha, "Towards realistic data generation for real-world super-resolution," *arXiv preprint arXiv:2406.07255*, 2024.

[16] L. Peng, A. Wu, W. Li, P. Xia, X. Dai, X. Zhang, X. Di, H. Sun, R. Pei, Y. Wang *et al.*, "Pixel to gaussian: Ultra-fast continuous super-resolution with 2d gaussian modeling," *arXiv preprint arXiv:2503.06617*, 2025.

[17] X. Guo, X. Wang, X. Fu, and Z.-J. Zha, "Deep unfolding network for image desnowing with snow shape prior," *IEEE Transactions on Circuits and Systems for Video Technology*, 2025.

[18] Y. LeCun, B. Boser, J. Denker, D. Henderson, R. Howard, W. Hubbard, and L. Jackel, "Handwritten digit recognition with a back-propagation network," *Advances in neural information processing systems*, vol. 2, 1989.

[19] A. Vaswani, N. Shazeer, N. Parmar, J. Uszkoreit, L. Jones, A. N. Gomez, Ł. Kaiser, and I. Polosukhin, "Attention is all you need," *Advances in neural information processing systems*, vol. 30, 2017.

[20] J. Ho, A. Jain, and P. Abbeel, "Denoising diffusion probabilistic models," *Advances in neural information processing systems*, vol. 33, pp. 6840–6851, 2020.

[21] B. Li, X. Liu, P. Hu, Z. Wu, J. Lv, and X. Peng, "All-in-one image restoration for unknown corruption," in *Proceedings of the IEEE/CVF conference on computer vision and pattern recognition*, 2022, pp. 17452–17462.

[22] V. Potlapalli, S. W. Zamir, S. H. Khan, and F. Shahbaz Khan, "Promptir: Prompting for all-in-one image restoration," *Advances in Neural Information Processing Systems*, vol. 36, pp. 71275–71293, 2023.

[23] J. Zhang, J. Huang, M. Yao, Z. Yang, H. Yu, M. Zhou, and F. Zhao, "Ingredient-oriented multi-degradation learning for image restoration," in *Proceedings of the IEEE/CVF conference on computer vision and pattern recognition*, 2023, pp. 5825–5835.

[24] Y. Cui, S. W. Zamir, S. Khan, A. Knoll, M. Shah, and F. S. Khan, "AdaIR: Adaptive all-in-one image restoration via frequency mining and modulation," in *The Thirteenth International Conference on Learning Representations*, 2025.

[25] Z. Luo, F. K. Gustafsson, Z. Zhao, J. Sjölund, and T. B. Schön, "Controlling vision-language models for universal image restoration," *arXiv preprint arXiv:2310.01018*, 2023.

[26] R. E. Kalman, "A new approach to linear filtering and prediction problems," 1960.

[27] L. Zhu, B. Liao, Q. Zhang, X. Wang, W. Liu, and X. Wang, "Vision mamba: Efficient visual representation learning with bidirectional state space model," *arXiv preprint arXiv:2401.09417*, 2024.

[28] A. Dosovitskiy, L. Beyer, A. Kolesnikov, D. Weissenborn, X. Zhai, T. Unterthiner, M. Dehghani, M. Minderer, G. Heigold, S. Gelly *et al.*, "An image is worth 16x16 words: Transformers for image recognition at scale," *arXiv preprint arXiv:2010.11929*, 2020.

[29] N. Yang, Y. Wang, Z. Liu, M. Li, Y. An, and X. Zhao, "Smamba: Sparse mamba for event-based object detection," *arXiv preprint arXiv:2501.11971*, 2025.

[30] C. Xiao, M. Li, Z. Zhang, D. Meng, and L. Zhang, "Spatial-mamba: Effective visual state space models via structure-aware state fusion," *arXiv preprint arXiv:2410.15091*, 2024.

[31] J. Sheng, J. Zhou, J. Wang, P. Ye, and J. Fan, "Dualmamba: A lightweight spectral-spatial mamba-convolution network for hyperspectral image classification," *IEEE Transactions on Geoscience and Remote Sensing*, 2024.

[32] H. Guo, J. Li, T. Dai, Z. Ouyang, X. Ren, and S.-T. Xia, "Mambair: A simple baseline for image restoration with state-space model," in *European conference on computer vision*. Springer, 2024, pp. 222–241.

[33] H. Guo, Y. Guo, Y. Zha, Y. Zhang, W. Li, T. Dai, S.-T. Xia, and Y. Li, "Mambairv2: Attentive state space restoration," *arXiv preprint arXiv:2411.15269*, 2024.

[34] L. Peng, X. Di, Z. Feng, W. Li, R. Pei, Y. Wang, X. Fu, Y. Cao, and Z.-J. Zha, "Directing mamba to complex textures: An efficient texture-aware state space model for image restoration," *arXiv preprint arXiv:2501.16583*, 2025.

[35] X. Di, L. Peng, P. Xia, W. Li, R. Pei, Y. Cao, Y. Wang, and Z.-J. Zha, "Qmambabsr: Burst image super-resolution with query state space model," *arXiv preprint arXiv:2408.08665*, 2024.

[36] Y. Wang, L. Peng, L. Li, Y. Cao, and Z.-J. Zha, "Decoupling-and-aggregating for image exposure correction," in *Proceedings of the IEEE/CVF conference on computer vision and pattern recognition*, 2023, pp. 18115–18124.

[37] L. Peng, Y. Cao, R. Pei, W. Li, J. Guo, X. Fu, Y. Wang, and Z.-J. Zha, "Efficient real-world image super-resolution via adaptive directional gradient convolution," *arXiv preprint arXiv:2405.07023*, 2024.

[38] L. Peng, Y. Cao, Y. Sun, and Y. Wang, "Lightweight adaptive feature de-drifting for compressed image classification," *IEEE Transactions on Multimedia*, vol. 26, pp. 6424–6436, 2024.

[39] S. W. Zamir, A. Arora, S. Khan, M. Hayat, F. S. Khan, and M.-H. Yang, "Restormer: Efficient transformer for high-resolution image restoration," in *Proceedings of the IEEE/CVF conference on computer vision and pattern recognition*, 2022, pp. 5728–5739.

[40] Y. Cui, W. Ren, X. Cao, and A. Knoll, "Focal network for image restoration," in *Proceedings of the IEEE/CVF international conference on computer vision*, 2023, pp. 13001–13011.

[41] D. P. Kingma and J. Ba, "Adam: A method for stochastic optimization," *arXiv preprint arXiv:1412.6980*, 2014.

[42] C. Wei, W. Wang, W. Yang, and J. Liu, "Deep retinex decomposition for low-light enhancement," *arXiv preprint arXiv:1808.04560*, 2018.

[43] S. Nah, T. Hyun Kim, and K. Mu Lee, "Deep multi-scale convolutional neural network for dynamic scene deblurring," in *Proceedings of the IEEE conference on computer vision and pattern recognition*, 2017, pp. 3883–3891.

[44] W. Yang, R. T. Tan, J. Feng, J. Liu, Z. Guo, and S. Yan, "Deep joint rain detection and removal from a single image," in *Proceedings of the IEEE conference on computer vision and pattern recognition*, 2017, pp. 1357–1366.

[45] X. Qin, Z. Wang, Y. Bai, X. Xie, and H. Jia, "Ffa-net: Feature fusion attention network for single image dehazing," in *Proceedings of the AAAI conference on artificial intelligence*, vol. 34, no. 07, 2020, pp. 11908–11915.

[46] K. Jiang, Z. Wang, P. Yi, C. Chen, B. Huang, Y. Luo, J. Ma, and J. Jiang, "Multi-scale progressive fusion network for single image deraining," in *Proceedings of the IEEE/CVF conference on computer vision and pattern recognition*, 2020, pp. 8346–8355.

[47] Y.-F. Liu, D.-W. Jaw, S.-C. Huang, and J.-N. Hwang, "Desnownet: Context-aware deep network for snow removal," *IEEE Transactions on Image Processing*, vol. 27, no. 6, pp. 3064–3073, 2018.

[48] J. Hai, Z. Xuan, R. Yang, Y. Hao, F. Zou, F. Lin, and S. Han, "R2rnet: Low-light image enhancement via real-low to real-normal network," *Journal of Visual Communication and Image Representation*, vol. 90, p. 103712, 2023.

[49] K. Ma, Z. Duanmu, Q. Wu, Z. Wang, H. Yong, H. Li, and L. Zhang, "Waterloo exploration database: New challenges for image quality assessment models," *IEEE Transactions on Image Processing*, vol. 26, no. 2, pp. 1004–1016, 2016.

[50] P. Arbelaez, M. Maire, C. Fowlkes, and J. Malik, "Contour detection and hierarchical image segmentation," *IEEE transactions on pattern analysis and machine intelligence*, vol. 33, no. 5, pp. 898–916, 2010.

[51] S. W. Zamir, A. Arora, S. Khan, M. Hayat, F. S. Khan, M.-H. Yang, and L. Shao, "Learning enriched features for real image restoration and enhancement," in *Computer Vision–ECCV 2020: 16th European Conference, Glasgow, UK, August 23–28, 2020, Proceedings, Part XXV 16*. Springer, 2020, pp. 492–511.

[52] L. Chen, X. Chu, X. Zhang, and J. Sun, "Simple baselines for image restoration," *arXiv preprint arXiv:2204.04676*, 2022.

[53] S. W. Zamir, A. Arora, S. Khan, M. Hayat, F. S. Khan, M.-H. Yang, and L. Shao, "Multi-stage progressive image restoration," in *CVPR*, 2021.

[54] M. Yao, R. Xu, Y. Guan, J. Huang, and Z. Xiong, "Neural degradation representation learning for all-in-one image restoration," *IEEE Transactions on Image Processing*, 2024.

[55] E. Zamfir, Z. Wu, N. Mehta, Y. Tan, D. P. Paudel, Y. Zhang, and R. Timofte, "Complexity experts are task-discriminative learners for any image restoration," 2024.

[56] W. Yang, R. T. Tan, J. Feng, Z. Guo, S. Yan, and J. Liu, "Joint rain detection and removal from a single image with contextualized deep networks," *IEEE transactions on pattern analysis and machine intelligence*, vol. 42, no. 6, pp. 1377–1393, 2019.

[57] Z. Tu, H. Talebi, H. Zhang, F. Yang, P. Milanfar, A. Bovik, and Y. Li, "Maxim: Multi-axis mlp for image processing," *CVPR*, 2022.

[58] Y. Jiang, X. Gong, D. Liu, Y. Cheng, C. Fang, X. Shen, J. Yang, P. Zhou, and Z. Wang, "Enlightengan: Deep light enhancement without paired supervision," *IEEE Transactions on Image Processing*, vol. 30, pp. 2340–2349, 2021.

[59] S. Nah, T. H. Kim, and K. M. Lee, "Deep multi-scale convolutional neural network for dynamic scene deblurring," in *The IEEE Conference on Computer Vision and Pattern Recognition (CVPR)*, July 2017.